

This is a research manuscript entitled “The miscibility of Calcium Silicate Perovskite and Bridgmanite: A single phase perovskite in hot, iron-rich regions” by Joshua M. R. Muir¹ (j.m.r.muir@mail.gyig.ac.cn) and Feiwu Zhang² (feiwuzhang@mail.gyig.ac.cn). This is a non-peer reviewed manuscript which has been submitted for publication in *Geochimica et Cosmochimica Acta*. Subsequent versions of this manuscript may have slightly different content. If accepted for publication the final version will be available via the Peer-reviewed publication link.

The miscibility of Calcium Silicate Perovskite and Bridgmanite: A single phase perovskite in hot, iron-rich regions

Joshua M. R. Muir¹, Feiwu Zhang²

Institute of Geochemistry, Chinese Academy of Sciences, 99 West Lincheng Road, Guiyang, Guizhou 550081, China

1 j.m.r.muir@mail.gyig.ac.cn

2 zhangfeiwu@mail.gyig.ac.cn

Abstract

Calcium silicate perovskite and bridgmanite are two phases which coexist in the lower mantle but at some temperature will dissolve into each other to form a single phase. In this work we use DFT to calculate the temperature at which this occurs at 3 pressures- 25, 75 and 125 GPa. At these three pressures we find solubility of Ca in Mg of 0.41/0.52/0.92 % at 2000 K and 0.72/1.07/3.30 % at 2500 K and of Mg in Ca of 0.18/0.13/0.06 % and 0.37/0.43/0.65 % for the pure MgSiO_3 - CaSiO_3 system. We thus conclude that in the absence of other elements pyrolytic compositions of bridgmanite and Calcium silicate perovskite do not mix in the lower mantle but could mix near the bottom (~90 GPa) of hotter mantle patches such as potentially in LLSVPs.

We build a simple model to test the effects of other elements and find that a large concentration (>~1 atomic%) is needed of any element before miscibility is strongly affected. Of the elements likely to be present in these kinds of concentrations ferrous iron increases miscibility while aluminium decreases it and ferric iron can increase or decrease it. With expected Fe and Al compositions pyrolite mixes at around ~90 GPa along a lower mantle geotherm but will remain unmixed if the Fe partitions largely to ferropericlase. Harzburgitic compositions are predicted to mix throughout the lower mantle with sufficient iron while basaltic compositions are predicted to remain unmixed at both geotherm and slab temperatures. We suggest therefore that phase mixing of Calcium silicate perovskite and bridgmanite is likely to be important in deeper, hotter and more iron enriched parts of the lower mantle.

Using static (~ 0 K) calculations we also predict that phase mixing of the perovskites will have strong seismic effects. For a pyrolytic mixture these are a small decrease in density (-0.14-0.25%), a significant decrease (-1.5-3.5%) in V_s , a small decrease in V_p (-0.5-1.2%) and a small increase in bulk sound (+0.00-0.75%). These seismic changes, while preliminary, are similar to those seen in LLSVPs which are also regions that are hotter and thus promote the formation of a single phase.

1. Introduction:

At depths of around 600-700 km perovskite (ABO_3) solutions will predominate in both ultra-mafic and mafic lithologies and control their physical attributes (Irifune and Ringwood, 1993, O' Neill and Jeanloz, 1990, Ono et al., 2004). In the lower mantle the two perovskite phases are $CaSiO_3$ (ca-pv) and $MgSiO_3$ (bdg). While work has been done to elucidate the seismic behaviour of both bdg (Ballaran et al., 2012) and ca-pv (Thomson et al., 2019) in order to understand their behaviour and effect on the lower mantle, these phases will not always exist as separate phases. With the same chemical formula Ca can replace Mg in bdg and Mg can replace Ca in Ca-pv and at sufficiently high temperatures the two phases will mix into a single phase. As this phase will have different seismic properties from a mechanical mixture of the individual phases it is essential to establish whether this two-phase chemical mixing is possible in lower mantle conditions.

The solubility of Ca into bdg and Mg into Ca-pv has been studied experimentally and it has generally been found that there is only a small solubility of these phases into each other at lower mantle conditions (Irifune et al., 2000, Irifune et al., 1989, Tamai and Yagi, 1989, Vitos et al., 2006, Jung and Schmidt, 2011, Fujino et al., 2004, Armstrong et al., 2012). This small solubility has been argued to derive from the large difference in size between Mg^{2+} and Ca^{2+} which impairs miscibility (Kesson et al., 1995, Vitos et al., 2006, Jung and Schmidt, 2011). At 25 GPa and ~ 2000 K Irifune et al. (2000) found that around 1-1.5% Ca-pv could dissolve in bridgmanite and 2.1-3.2% bdg in Ca-pv while at 30 GPa and 2000-2300 K Fujino et al. (2004) found around 1% and 4% respectively. In Armstrong et al. (2012) it was found that up to 46 GPa and 2000 K only 5% Ca could be dissolved into bdg whereas for Mg in Ca-

pv solubility was found to be less than 5% at 30 GPa but over 10% at 55 GPa and 2000 K. Theoretically Jung and Schmidt (2011) found the solubility of Ca in bdg to be ~0.5 % and that the solubility of Mg in Ca-pv was much lower at 2000 K and 25 GPa while Vitos et al. (2006) found this solubility to be around an order of magnitude higher. In both theoretical papers solubility decreased with pressure in contrast to experimental results (Armstrong et al., 2012, Fujino et al., 2004) which find that solubility increases strongly with pressure. In both theoretical and experimental cases solubility increases markedly with temperature.

From the studies of Irifune et al. (2000), Fujino et al. (2004) and Armstrong et al. (2012) it is clear that at the top of the lower mantle Ca-pv and bdg exist as separate phases. The strong pressure dependence on mixing seen in Fujino et al. (2004) and Armstrong et al. (2012) however, suggests that deep within the lower mantle, beyond the pressures and temperatures of these experiments, the two phases could be miscible. Thus determining the miscibility of these two phases at the high temperatures and pressures of the lowermost mantle is essential for determining their phase structure. It is also important to resolve the different predictions of the effect of pressure on solubility that have been seen between experimental and theoretical works.

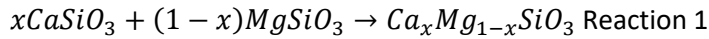
Another factor which needs to be considered is the presence of contaminants and their effect on phase miscibility. Both Ti (Armstrong et al., 2012) and Fe (Fujino et al., 2004) have been shown to increase the mixing of these two phases but it is unclear what elements are important and how big of an effect these elements have on the overall miscibility.

Thus in this work we shall use Density Functional Theory (DFT) to probe the solubility of Ca-pv and bdg in each other up to D'' pressures and temperatures (125 GPa and 3000 K) and in the presence of a variety of elements. This shall allow us to build a model of Ca-pv and bdg miscibility and speculate as to where in the lower mantle these two phases are mixed. We shall then also estimate the seismic effects of this mixing.

2. Methods

Mixing Thermodynamics

To determine whether two phases mix we simply need to determine the energy of the following reaction:



Reaction 1 is for the pure end members. Defect elements can be introduced by adding them to both sides of the reaction.

The energy of this mixing reaction can be represented by:

$$G_{Mix} = H_{Mix} - TS_{Mix} \text{ Equation 1}$$

where H_{mix} is the enthalpy of mixing, T is the temperature, S_{mix} is the entropy of mixing and G_{mix} is the free energy of mixing. Mixing will occur when G_{mix} is negative. S_{mix} will be broken into two components- S_{vib} a component representing vibrational entropy and S_{config} a component representing configurational entropy. G_{mix} will then be determined in two parts. H_{mix} and S_{vib} will be determined through molecular dynamics and S_{config} will be determined through static calculations.

To determine mixing over an array of conditions we ran calculations at various points and extrapolated between them. For the molecular dynamics portions we ran calculations at 25, 75 and 125 GPa and at 1000, 2000 and 3000 K. All pressures are uncorrected. Energies were determined at Ca%=0, 25, 50 and 100 where Ca% is $Ca/(Ca+Mg)$.

To calculate G_{mix} at any arbitrary T , P and Ca% we then used the following scheme. First at each pressure point (25, 75 and 125 GPa) and at each Ca% point (0, 25, 50 and 100) we calculated G of the products and the reactants as a function of T . We then fit polynomials as a function of T and determined the G of the products and the reactants at the T of interest. We then fit polynomials as a function of Ca% and then pressure and calculated G_{mix} at the appropriate Ca% and pressure in this order. The fits across P and T are relatively linear and are likely reliable. Energy varies strongly as a function of Ca% and inaccuracies in Ca% extrapolation could lead to large errors in G_{mix} . The G of the points at Ca%=25 fit near exactly to a curve of G vs Ca% plotted with points at Ca%=0, 50 and 100 as

shown in Figure S1 which suggests that a polynomial fit of G vs $\text{Ca}\%$ is adequate. This fitting likely breaks down at extremely high and low $\text{Ca}\%$ values but these values are not geophysically interesting.

Computational Details

For these calculations we used the VASP code version 5.4.4 (Kresse and Furthmuller, 1996b, Kresse and Furthmuller, 1996a). This is a density functional theory approach where planewave pseudopotentials are used to simulate supercells which represent infinite crystals. The PBE (Perdew et al., 1996) exchange correlation functional was used alongside the included VASP PAW potentials (Kresse and Joubert, 1999). The valence electron shells used were Ca: 3s, 3p, 4s; Mg 3s, 3p; Si 2s, 2p; O 2s, 2p. Two different sets of calculations were performed, static and molecular dynamics. Static calculations had planewave cutoffs of 850 eV, k-point grids of $4 \times 4 \times 4$ in a Monkhorst Pack grid (Monkhorst and Pack, 1976). Energies were relaxed to within 10^{-5} eV and forces between atoms were relaxed to below 10^{-4} eV/Å. For molecular dynamic runs the gamma point was used with cutoffs of 600 eV and relaxed to within 10^{-4} eV. 80 atom unit cells were used ($2 \times 2 \times 1$) except for the configurational entropy as noted below.

To calculate the elasticity of our components we used static calculations with the cutoffs listed above. We used 80 atom unit cells and a mixed phase that had $\text{Ca}\%=12.5$ ($\text{Mg}_{14}\text{Ca}_2\text{Si}_{16}\text{O}_{48}$). Elasticity was calculated by applying small stresses to the cell and plotting the responding strain. We used an online script (<https://github.com/andreww/elastic-constants>) to ease calculation. In each case 4 strain points were used corresponding to 0.01, 0.02, -0.01 and -0.02.

Phases:

Multiple different phases are possible in this system. MgSiO_3 is usually in the orthorhombic pbnm phase (Zhang et al., 2013) while CaSiO_3 is in the cubic $\text{pm}3\text{m}$ or the tetragonal $\text{i}4\text{mcm}$ phase (Stixrude et al., 2007, Sun et al., 2014). All systems (end members and mixtures) were calculated in all 3 of these phases. All extrapolations across $\text{Ca}\%$ and temperature were done for all 3 phases and then at any specific composition and temperature point the lowest energy phase was chosen. For Mg end members pbnm phases dominated, for Ca end members $\text{i}4\text{mcm}$ or $\text{pm}3\text{m}$ phases were dominant with

pm3m phases favoured by high temperatures. The single mixed phase generally adopts a pbnm structure with this always being adopted when Ca%=25 or 50. This preference for a pbnm structure in the mixed phase was also observed experimentally by Armstrong et al. (2012) and theoretically by Jung and Schmidt (2011).

It should be noted that simulating the phase of CaSiO₃ has proven very difficult in the past- see for example (Kawai and Tsuchiya, 2015, Stixrude et al., 2007, Sun et al., 2014). This is for two reasons. The first is then the pm3m phase is not stable at static conditions and thus possesses imaginary frequencies which prevents the use of quasi-harmonic approximations. We avoid this problem by using molecular dynamics. The second issue is that the phases are often close in energy and simulations can often sample phonons from the other phases. This is less of a problem in this work as we only use the energy of the most stable Ca-pv phase at any point and do not care about determining exactly which phase is actually stable. The energy difference between i4mcm and pm3m for CaSiO₃ was always found to be < 6 meV/atom which is very small compared to the values of G_{mix} and thus it is difficult to determine which phase is stable but much easier to determine the energy of these Ca-pv phases relative to the Mg and mixed phases.

To test whether post-perovskite phases were promoted by phase mixing, calculations were run on a mixed phase with a cmcm structure and Ca%= 50 at 125 GPa but this post perovskite phase was found to be higher in energy than the pbnm phase at all tested temperatures (1000, 2000 and 3000 K).

Molecular Dynamics:

To determine the vibrational entropy we used a Velocity-Autocorrelation Function (VACF) method. More accurate methods such as thermodynamic integration are possible but as G_{mix} values are fairly large the extreme accuracy of these methods is likely unnecessary. To determine vibrational entropy we first need the vibrational density of states function S(v) which represents the distribution of normal modes (v) in the system. This can be represented as:

$$S(v) = \frac{2}{k_b T} \sum_{i=1}^N \sum_{k=1}^3 m_i s_i^k \text{ Equation 2}$$

where N is the total number of atoms in the system, m_i is the mass of atom i , s_i^k is the spectral density of atom i in the direction k ($x=1, y=2, z=3$), T is the temperature and k_b is the Boltzmann constant. In our case s_i^k is obtained by taking the fourier transform of the VACF. Entropy is then obtained by

$$S_{vib} = k_b \int_0^{\infty} S(\nu) d\nu \text{ Equation 3}$$

Entropies and enthalpies were determined from molecular dynamics runs with a length of 2.5 ps. Running the molecular dynamics for 1, 1.5 and 2 ps did not provide sufficient accuracy in energy but the energies obtained from 2.5 ps runs were replicated (within 2 meV/atom) by 4 ps runs in selected systems.

The error of the energies obtained from molecular dynamics were calculated for each individual run using the method of Flyvbjerg and Petersen (Flyvbjerg and Petersen, 1989) and were less than 1.5 meV/atom in all cases. Propagating these errors leads to the error in mixing temperatures being <30 K (2σ) and <70 K (2σ) for pyrolytic mixtures but these are likely underestimates as some fitting errors may be unaccounted for.

Configurational Entropy:

To determine the configurational entropy of mixed phases we calculated the energy of different configurations of Mg and Ca in the unit cell. As the number of configurations increase with N factorial 80 atom unit cells proved too large to obtain a workable number of configurations. The energy difference of different configurations is independent of unit cell size, however, and the disadvantage of using a small unit cell in these calculations is simply that some configurations may not be appropriately sampled. To this end for $\text{Ca}_x\text{Mg}_{1-x}\text{SiO}_3$ where $x=0.5$ or $x=0.25$ (0.75) we determined configurational entropy in a 40 atom unit cell ($2 \times 1 \times 1$). This 40 atom unit cell will not contain every configuration possible in larger cells but contains a large sample of different configurations and thus should adequately approximate the configurational entropy of an infinite cell. For $x=0.125$ (0.875) an 80 atom unit cell was used as the 40 atom unit cell only provides 1 unique configuration.

For $\text{Ca}_x\text{Mg}_{1-x}\text{SiO}_3$ we first determined the number of unique configurations for $x=0.125, 0.25, 0.5, 0.75$ and 0.875 . These structures have 120, 28, 70, 28, 120 total configurations respectively of which 9, 5, 10, 5, 9 are unique. At $x=0$ and $x=1$ S_{config} is 0 by definition. The energy of each of these configurations was calculated statically at 25, 75 and 125 GPa. To determine S_{config} we then used the Gibbs entropy formulation:

$$Z = \sum_i e^{\frac{-E_i}{k_b T}} \text{ Equation 4}$$

$$P_i = \frac{1}{Z} e^{\frac{-E_i}{k_b T}} \text{ Equation 5}$$

$$S_{\text{config}} = -k_b \sum_i p_i \ln p_i \text{ Equation 6}$$

where Z is the partition function, i is each configuration (including degenerate copies of each configuration), E_i is the energy of that configuration and p_i is the probability that it occurs. If every configuration has equivalent energy these calculations reduce to the Boltzmann entropy formula which is ideal mixing of Ca and Mg in these systems. S_{config} was then projected using a polynomial across Ca% and added to the other terms derived from MD in Equation 1.

3. Results:

Enthalpy and Entropy of Mixing

The mixing of two naturally immiscible substances can be represented by Equation 1. For two naturally immiscible substances H_{mix} will be positive because the two substances don't naturally mix and S_{mix} will be positive because there are more ways of arranging a mixed phase than 2 separate individual phases. Mixing occurs when G_{mix} is negative. As S_{mix} is multiplied by $-T$ as temperature increases G_{mix} will gradually decrease and at some temperature $-TS_{\text{mix}}$ will equal H_{mix} , $G_{\text{mix}}=0$ and mixing occurs. We will refer to this temperature as T_{mix} and it is equivalent to the phase boundary temperature between 1 (mixed) and 2 (unmixed) phase regions of Ca-pv and bdg.

H_{mix} is shown as a function of pressure in Figure 1, S_{config} and S_{vib} are shown in Tables 1 and 2. With increasing pressure H_{mix} increases, S_{config} has a small increase but is effectively unchanged and S_{vib} has

a more complex relationship but generally increases with pressure. H_{Mix} increases with pressure despite the mixture being less dense than a manual mixture of two phases (Table 3). This increase is most likely due to the difficulty of placing a large Ca^{2+} ion in a small Mg^{2+} cavity as this gets more difficult with pressure as the Mg^{2+} cavity gets smaller.

Increasing H_{Mix} increases T_{mix} but increasing S_{Vib} decreases T_{mix} and the increase in S_{Vib} is much larger than the increase in H_{Mix} . Thus with increasing pressure T_{mix} should decrease as has been observed by Fujino et al. (2004) and Armstrong et al. (2012) and this decrease is due to changes in S_{Vib} . This reliance on S_{Vib} to decrease T_{mix} with increasing pressure explains why the two earlier theoretical studies (Jung and Schmidt, 2011, Vitos et al., 2006) observed an increase in T_{mix} with pressure as these studies estimated S_{Vib} and did not calculate it. These studies also observed very high T_{mix} (>4000 K) values which are much larger than those reported in experiments. This discrepancy has the same cause. As shown in Figure 1 without S_{Vib} calculated T_{mix} values are extremely high and increase with pressure but as seen in Figure 2 when we include S_{Vib} T_{mix} values drop substantially and decrease with pressure.

S_{config} has some variation from its ideal Boltzmann entropy value but this is small- replacing our S_{config} values with those of an ideal Boltzmann mixture causes changes in T_{mix} of less than 75 K in all cases and generally less than 10 K. Thus we conclude that Ca and Mg are largely interchangeable on different sites (ideal mixing) as far as configurational entropy is concerned.

Mixing in the CaSiO_3 - MgSiO_3 system:

Figure 2 shows the solubility of Ca in bdg and Mg in Ca as a function of temperature at 25, 75 and 125 GPa. In each case we find two regions in the solubility curve. First at low or high Ca% (where Ca% is $\text{Ca}/(\text{Ca}+\text{Mg})$) increasing the temperature leads to sharp increases in solubility- this region is predominantly controlled by H_{mix} and S_{Vib} . At middling Ca% values there is a plateau in the solubility vs temperature response and this region is controlled by S_{config} . As S_{config} reaches its maximum when the Ca% value is 50 increasing the solubility in this region does not require an increase in temperature

and hence the plateau. Once the plateau temperature is reached then all ratios of Ca-pv and bdg can be mixed and Ca-pv and bdg will always dissolve into each other.

In the $\text{CaSiO}_3\text{-MgSiO}_3$ system we find the solubility of Ca in bdg to be $\sim 0.41\%$ and of Mg in Ca-pv to be $\sim 0.18\%$ at 2000 K and 25 GPa while the plateau T_{mix} is ~ 3170 K. At 75 GPa we find the solubility to be ~ 0.52 and $\sim 0.13\%$ at 2000 K and the plateau T_{mix} to be ~ 3050 K. At 125 GPa we find the solubility to be ~ 0.92 and $\sim 0.06\%$ at 2000 K and the plateau T_{mix} to be ~ 2740 K. With increasing pressure solubility at 2000 K is not strongly varied but at higher temperatures pressure has a very large effect on solubility as seen by the differing plateau T_{mix} temperatures. In the theoretical study of Jung and Schmidt (2011) the solubility of Ca in bdg was found to be 0.5% and the solubility of Mg in Ca-pv to be much lower at 25 GPa which is similar to our work.

Experimentally Fujino et al. (2004) found solubilities of 1% Ca in bdg and 4% Mg in Ca-pv at 2273 K and 30 GPa, Irifune et al. (2000) found 1.1-1.5% solubility of Ca in bdg and 2.1-3.2% of Mg in Ca-pv at 25 GPa and 1973 K and Armstrong et al. (2012) found 4.7% solubility of Mg in Ca-pv at 53 GPa and 2000 K. These experimental results all show higher solubility than we predict here. Small solubilities are the hardest to constrain as they occupy the steepest part of Figure 2. Small errors in our calculations or in the experiments could easily lead to such differences, solubilities on the order of mantle phase compositions should be much better constrained. These discrepancies could also be explained with experimental temperatures being higher than recorded or by the presence of impurities the possible effects of which we shall explore in the next section.

The Effect of Other Elements

Ca-pv and bdg can contain many other defect elements in the mantle. Bridgmanite crystals typically contain large (1-10%) amounts of iron and Al (Kaminski, 2017) and potentially many other elements. Even elements that are present in extremely small amounts will have large effects on S_{Config} while elements present in large amounts will have effects on H_{mix} and S_{vib} . We have no conceptual model for which elements could affect the mixing parameters and so instead we tested a large number of

elements as shown in Table 4 (for 25 GPa and 125 GPa and Ca%=10, a roughly pyrolytic mixture). To test the effect of a large number of atoms we used a simple model with a few assumptions.

- 1) That S_{vib} is unaffected by the addition of defects. S_{vib} is dependent on long-range phonons and thus is likely unaffected by small additions but could be strongly affected by defects that are present in large quantities like Fe. Thus we are only calculating changes to H_{mix} (through static calculations) and S_{config} .
- 2) That S_{config} is perfect when considering additional defects. S_{config} changes are therefore solely dependent upon the number of sites in the system.
- 3) That the addition of defects affects H_{mix} linearly- ie adding 2 iron atoms has twice the energy of adding 1 iron atom.
- 4) That defect elements are confined to a single type of site and either replace a Mg, a Si, both a Mg and a Si or exist in their most stable interstitial site as shown in Table 4.
- 5) That defect elements are partitioned before phase mixing entirely into the bdg or the ca-pv phase (depending upon energy).

While all five of these assumptions will break down, particularly at large concentrations of defects, with this method we can capture two of the largest energy changes induced by defect elements (S_{config} and H_{mix}) and thus determine broadly what types of elements are most important for Ca-pv and bdg mixing. To test how accurate these assumptions are, we performed more explicit calculations upon one defect element Ti. The full results and method of this will be presented in future work but in essence we explicitly calculated S_{config} and S_{vib} through the same methods as above but for a range of Ti% (Ti/(Ti+Si)) values (0, 25, 50, 100). A comparison between the full calculation and the simple model presented above is given in Table 5. While there are significant differences between our actual results and our simple model our simple model correctly predicts the magnitude of results and thus it should predict both which elements are important for inducing mixing and the concentration that these elements need to appear in to be significant.

As can be seen in Table 4 there is no clear trend in the effect of defect elements on T_{mix} with either charge or ionic size and thus individual electronic effects are very important. This makes it hard to predict off-hand which elements will effect T_{mix} in what way. Some elements reduce H_{mix} and thus also T_{mix} . The most important of these are the noble gases (which can cause very large reductions of H_{mix} due to their position as an interstitial defect), Na(I), K(I), many of the transition metals in particular Co(II), Ni(II) Sc(II) and Fe(II), and 4+ cations that replace Si such as S, Ti and C. Some elements that strongly increase H_{mix} and thus T_{mix} are the larger alkaline earth metals (Sr, Ba) and B. Increasing the pressure has varied effects on these trends increasing H_{mix} for some elements and decreasing it for others but defect induced ΔT_{mix} values are similar at 25 and 125 GPa. This is because the largest effect of defect elements on T_{mix} is through modifying S_{config} which in this model is pressure independent. Even though defect changes to H_{mix} (ΔH_{mix}) are very significant, pressure induced changes to ΔH_{mix} are largely insignificant compared to S_{config} .

The most notable trend, however, is that large amounts of defects are required to induce significant changes in T_{mix} . With Ca%=10 for all atoms a concentration of at least 0.3 atomic% is required to change T_{mix} by 100 K with the required concentration being over 1 atomic % for most elements. This is significant because most defects in bridgmanite and likely Ca-pv are well below this level. This means we can restrict our consideration of these defect element effects to either highly chemically heterogeneous regions or to those defects that are likely to be present in large numbers in the lower mantle- primarily Fe and Al.

Fe is present in bridgmanite in concentrations of around 5-10% and is predominantly ferrous and high spin (Shim et al., 2017, Xu et al., 2015, Shukla et al., 2015). High spin ferrous Fe decreases T_{mix} by up to 1000 K (Fe%=10 Ca%=10) in a pyrolytic mixture. Fujino et al. (2004) observed that adding iron increased the total solubility at a fixed temperature. Al on the contrary increases T_{mix} by up to 230 K (Al%=5 Ca%=10) and so counteracts the effects of Ferrous iron somewhat. The presence of Al can also oxidise ferrous to ferric iron by forming Fe-Al pairs where the iron exists as high spin on (primarily) the A site (Shim et al., 2017, Catalli et al., 2011, Kuppenko et al., 2014). With the introduction of Fe-Al pairs

T_{mix} is largely unaffected with T_{mix} changing by -38 K with Fe-Al%=5 and Ca%=10. Pure ferric iron slightly decreases T_{mix} at low pressure and slightly increases it at high pressure.

The effect of these elements on some non-pyrolytic mixtures is shown in Table S1 and S2. As Ca% approaches 50 these defect element effect typically decrease such that for a Ca%=50 mixture the value of ΔT_{mix} is roughly half of what it would be in an equivalent pyrolytic system. This relationship, however, breaks down when the change in H_{mix} caused by defect elements is very low or very high such as with pure ferric iron. The effect of defect elements on mixtures with high Ca% is similar to those with low Ca% but generally larger. This is a potential explanation of the higher solubilities of high Ca% solutions compared to low Ca% solutions (Armstrong et al., 2012, Fujino et al., 2004, Irifune et al., 2000) that has been seen in the literature previously but is in contrast to our calculations. Any defective elements that were present in the experiment would have the effect of raising the solubility of the high Ca% solutions more than the low Ca% solutions.

Discussion:

Single phase regions of the lower mantle

In the lower mantle Ca% can have various values. For pyrolytic mantle it is generally been 7-12% (Kesson et al., 1998, Irifune and Tsuchida, 2007, Mattern et al., 2005, Ringwood, 1991), for a harzburgitic mantle it is ~1-3% (Ringwood, 1991, Michael and Bonatti, 1985) and for a subducted mid-ocean range basalt (MORB) it is between 40-60% (Hirose et al., 2005, Hirose and Fei, 2002, Irifune and Tsuchida, 2007, Ricolleau et al., 2010). In defect-free pyrolytic or MORB mantle the exact value of Ca% in these ranges does not matter because the difference in T_{mix} between the high Ca% and low Ca% value in this range is very small (30 K and 5 K for defect-free pyrolytic and MORB respectively at 25 GPa). For harzburgitic mantle the exact value of Ca% is very important because the difference between T_{mix} for Ca%=1 and Ca%=3 for example is 320 K at 25 GPa as this Ca% range occurs during the steep change in solubility (Figure 2).

Pyrolytic Compositions

The T_{mix} of these mixtures vs some lower mantle temperatures using an extrapolation of our model is shown in Figure 3 for a pyrolytic composition, Figure 4 for a MORB composition and Figure 5 for a harzburgitic composition. When the temperature exceeds T_{mix} these solutions will mix into a single phase. For a pure pyrolytic composition with no additional elements we see that it remains above the lower mantle geotherm up until the D'' at 125 GPa. Thus pure CaSiO_3 and MgSiO_3 will not mix along a standard mantle geotherm. Hot spots in the mantle, such as in mantle plumes or LLSVPs, can cause this phase to mix however. Shown in Figure 3 is a geotherm with an excess temperature of 500 K as is possible in LLSVPS or plumes (McNamara, 2019). At this excess temperature mixing of the pure phases should begin around 80 GPa and thus anomalously hot regions of the mantle should see phase mixing of Ca-pv and bdg near their lower depths.

The addition of defect elements that are likely to exist at these depths furthers this case. While our results for Al and Fe have significant assumptions and need more testing they should correctly predict the sign of ΔT_{mix} and its rough magnitude. With a standard composition of 8% Fe^{2+} , 2% Fe^{3+} - Al^{3+} mixing now occurs at ~ 85 GPa along the geotherm and ~ 45 GPa on the elevated geotherm. With an alternative composition of 10% ferrous iron and 5% Al mixing occurs at ~ 95 and ~ 60 GPa respectively. With a heavily aluminous or aluminous-ferrous composition T_{mix} is increased so that mixing does not occur along either of these temperature profiles. With a heavily iron enriched composition (such as 20% Ferrous iron, 5% Al), such as may occur in ULVZs, mixing is heavily enhanced.

These iron induced mixed phases are less likely to form in real mantle however. In our work we have ignored the effects of periclase. While periclase should have no effect on the mixing reaction directly it could partition elements out of the perovskites and thus make them unable to affect mixing. Periclase usually partitions iron out of bridgmanite (Muir and Brodholt, 2016). Thus bridgmanite in the lower mantle will generally not have large amounts of iron and so T_{mix} should remain somewhere near the "perfect" values in Figure 3 and mixing should not occur.

As seen in Figure 3 while the Ca% ratio is largely unimportant in mixing pure pyrolytic phases when defect elements are present it becomes very important. Across a standard pyrolytic range of Ca%=7-

$12 T_{\text{mix}}$ can vary by 500 K when defect elements are present. This is due to the introduction of different S_{config} terms. This suggests that in highly chemically heterogeneous regions variations in Ca as well as more minor defect elements are important.

One area of the mantle that potentially has a compositional difference is LLSVPS (McNamara, 2019). While it is unclear what this compositional difference is, as shown in Table 4 only differences that exceed ~ 1 atomic% are important to mixing of the perovskites. It is unlikely that LLSVPs contain any defective element in this concentration that is not Fe or Al. Thus when considering LLSVPs mixing of the perovskite phase should primarily be constrained by their elevated temperature with a secondary effect for potential changes in Fe and Al content. Any exotic compositional differences that may exist are unlikely to be important for phase mixing of the perovskite. As LLSVPs are considerably hotter than the rest of the mantle they should thus likely possess some perovskite phase mixing as should other hot areas of the mantle.

One area where this mixing behaviour is potentially important is in the formation of a post-perovskite (ppv) phase in bdg and hence on the D'' . As the pressure increases beyond 125 GPa the free energy of the single chemically mixed phase (Ca-pv+bdg) becomes lower than the free energy of the mechanically mixed Ca-pv+bdg phases and this is particularly the case with additional iron. This is important because it means that the addition of Ca-pv at D'' conditions stabilises the bdg phase against the ppv phase unless Ca can similarly dissolve into a ppv phase which has been suggested to be unlikely in the literature (Fujino et al., 2009). As discussed in the methods we find a ppv analogue in the mixed phase to be unstable compared to a bdg perovskite (pv) analogue which is additional evidence that Ca-containing structures do not like to form ppv structures. Thus we must consider how the stabilisation of the perovskite mixed phases compares to the stabilisation of the bdg post-perovskite phase.

To examine whether this is an important effect we compared the energies of G_{mix} vs literature energies for the pv to ppv transition of bdg. To obtain energies for this latter transition we took the Clapeyron slope (9.56 MPa/K) and volume difference (1.78 Å³) of the pv to ppv transition in bdg from

Oganov and Ono (2004) and converted these to an energy difference of ~ 1.06 meV/Kf.u. between the pv and ppv phase. At 127 GPa and 3000 K (a rough value for the point where pv converts into ppv in pure bdg) G_{mix} is 23.5 meV/f.u. for a pure mixture and 8.94 meV/fu for a mixture with 8% ferrous iron and 2% Fe-Al mixture. These values correspond to a stabilisation of the bridgmanite phase relative to the post-perovskite phase of ~ 2.1 and 0.8 GPa respectively. These numbers are significant for pure bridgmanite but are small when compared to the effects of other elements (Grocholski et al., 2012) and thus the Ca% ratio is likely to be only a minor control on this reaction in the real mantle.

Harzburgitic Compositions

Predicted mixing temperatures of harzburgite are shown in Figure 4. Harzburgitic compositions behave largely like pyrolytic compositions but they have smaller T_{mix} values and thus mix at shallower depths. Varying the Ca% ratio has an even larger effect on T_{mix} in harzburgite than in pyrolite because the possible Ca% values exist in an even steeper range of the solubility curve. A perfect mixture mixes along the geotherm at 115 GPa, a 10% ferrous iron and 5% Al mixture at 105 GPa and a 8% ferrous iron 2% Fe-Al mixture is mixed throughout the lower mantle and even mixes in the coldest slabs.

Basaltic Compositions

A final case to consider is a descending slab with a more MORB-like composition. This has quite different behaviour to the pyrolytic case and is shown in Figure 5. T_{Mix} is considerably higher in the MORB case and is considerably above the temperature of descending slabs (the coldest slab adiabat is shown in Figure 5). Varying the Ca% ratio has little effect on mixing in basaltic compositions as they exist in the plateau region of Figure 2 and thus all basaltic compositions should behave largely similarly. Even in the case of extremely enriched iron (20%) T_{Mix} remains nearly 600 K above the temperature of the coldest adiabat at 125 GPa and thus phase mixing does not occur in descending slabs even in cases of extreme iron enrichment.

While we predict no mixing in the lower mantle for MORB our predicted mixing temperatures for MORB contradict an experimental study where MORB was heated until it melts at varying pressures up to CMB pressures and no sign of phase mixing was observed in the XRD spectra (Pradhan et al., 2015). While this sample contains large amounts of Al which will increase T_{mix} our predicted T_{mix} is still well below the melting temperature at high pressure. In this study samples were heated for 30 minutes which is similar to the heating times for experiments where mixing has been observed (Armstrong et al., 2012, Fujino et al., 2004, Irifune et al., 2000). This suggests generally that mixing had enough time to occur in these melting experiments and the lack of any mixed phase formation was not a kinetic effect. One possible solution to this is that these melting experiments had large amounts of Fe and Al when compared to the other studies and these elements would need to diffuse before and during mixing which could delay the formation of a single phase as this diffusion is slow. Alternatively our simple model may underestimate the effect of some elements, most likely Al, in raising T_{mix} and the full effect of these elements needs to be modelled with MD or experimentally.

Seismic Effects

We have established that the 2 phases Ca-pv and bdg mix in chemically anomalous or hot and deep parts of the lower mantle. It is important now to consider what seismic effects if any this mixing will have.

Table 3 shows the density of the mixed phase as compared to a mechanical mixing of the two phases for a pyrolytic mixture. The mixed phase is less dense than a mechanical mixture of the other two phases but this change is small (<0.26%) and thus is unlikely to have large dynamic effects. In Figure 6 we consider the elasticity of these structures. This is a difficult problem for multiple reasons. First the elasticity of the Ca-pv phase has proven to be difficult to measure both theoretically and experimentally (Thomson et al., 2019, Kawai and Tsuchiya, 2015). Second any consideration of elasticity differences also needs to account for possible temperature differences between 2 and 1 phase regions in the mantle as well as possible phase changes. Third the elasticity of a mechanical

mixture of Ca-pv and bdg depends upon the geometry of its mixing and without this knowledge large bounds exist. We shall however estimate the elasticity difference between a chemically mixed and a mechanically mixed phase by using static calculations (elasticity at ~ 0 K). To account for the third point our mechanical mixture of Ca-pv and bdg shall be a Hashin-Shtrikman mixture which provides the maximum and minimum possible bounds on elasticity regardless of mixing geometry (Hashin and Shtrikman, 1963).

Using these approximations we find that chemically mixing the two phases causes a drop in V_s of -1.5-3.5%, a drop in V_p of -0.5-1.2% and an increase in V_ϕ of 0.0-0.75% when compared to a mechanical mixture of the two phases. These changes are seismically relevant and are similar to those of LLSVPs where a drop in V_s of $\sim 2\%$, a small change to density that is possibly positive or negative and anticorrelation of V_s and bulk sound speed have all been observed (McNamara, 2019). Anticorrelation of V_s and bulk sound is uncommon as both V_s and bulk sound are proportional to the inverse square root of density so that even moderate changes in density will cause them both to vary in the same direction regardless of K and G changes. This relationship puts strong limits on the possible density variations of LLSVPs and modelling of LLSVPs agrees with this assessment as density variations between LLSVPs and bulk mantle are predicted to be small. Such assessments place strong limits on the range of compositional variations that could lead to LLSVPs as enrichments of elements like Fe should cause strong density variations. As demonstrated here structural changes of the underlying minerals which sometimes lead to only small density variations are potentially much more likely and can lead to anticorrelation.

To draw strong conclusions, however, work on the elasticity of the mixed phase at high temperature needs to be performed. As we demonstrate above correctly determining the mixing temperature requires high temperature calculations and thus high temperature phonons might also have a strong effect on elasticity.

Conclusion

In this work we find that Ca-pv and bdg are unlikely to mix in the lower mantle in the absence of additional elements but will mix near the lower end of the mantle in the case of elevated temperatures such as in an LLSVPs. Descending slabs should remain as two phases in all cases.

Using a simple model we demonstrate that only defects with large concentration affect mixing of these phases. Of the most likely elements that meet this requirement ferrous iron increases mixing, aluminium decreases it and ferric iron can increase or decrease it. With a likely pyrolytic composition mixing is increased and phase mixing occurs at ~85 GPa along a geotherm if iron remains in the perovskite phase and does not partition to periclase.

This mixing will lead to small density decreases alongside a seismically significant decrease in shear wave speed and anticorrelation with the bulk sound speed. These elasticity changes are similar to those predicted for LLSVPs and the excess temperatures of LLSVPs also makes phase mixing more likely. Some significant approximations have been made to estimate elasticity and the effect of Fe and Al, however, and more work needs to be done on these points to address this.

Acknowledgments:

The research in this proposal was supported by National Natural Science Foundation of China (41773057). JM is highly thankful to Chinese Academy of Sciences (CAS) for PIFI. Calculations were run on the TH-2 High Performance Computer System in Lvliang, China.

Bibliography

- ARMSTRONG, L. S., WALTER, M. J., TUFF, J. R., LORD, O. T., LENNIE, A. R., KLEPPE, A. K. & CLARK, S. M. 2012. Perovskite Phase Relations in the System CaO-MgO-TiO₂-SiO₂ and Implications for Deep Mantle Lithologies. *Journal of Petrology*, 53, 611-635.
- BALLARAN, T. B., KURNOSOV, A., GLAZYRIN, K., FROST, D. J., MERLINI, M., HANFLAND, M. & CARACAS, R. 2012. Effect of chemistry on the compressibility of silicate perovskite in the lower mantle. *Earth and Planetary Science Letters*, 333, 181-190.

- CATALLI, K., SHIM, S.-H., DERA, P., PRAKAPENKA, V. B., ZHAO, J., STURHAHN, W., CHOW, P., XIAO, Y., CYNN, H. & EVANS, W. J. 2011. Effects of the Fe³⁺ spin transition on the properties of aluminous perovskite—New insights for lower-mantle seismic heterogeneities. *Earth and Planetary Science Letters*, 310, 293-302.
- EBERLE, M., GRASSET, O. & SOTIN, C. 2002. A numerical study of the interaction between the mantle wedge, subducting slab, and overriding plate. *Physics of the Earth and Planetary Interiors*, 134, 191-202.
- FLYVBJERG, H. & PETERSEN, H. G. 1989. Error-estimates on averages of correlated data. *Journal of Chemical Physics*, 91, 461-466.
- FUJINO, K., NISHIO-HAMANE, D., SUZUKI, K., IZUMI, H., SETO, Y. & NAGAI, T. 2009. Stability of the perovskite structure and possibility of the transition to the post-perovskite structure in CaSiO₃, FeSiO₃, MnSiO₃ and CoSiO₃. *Physics of the Earth and Planetary Interiors*, 177, 147-151.
- FUJINO, K., SASAKI, Y., KOMORI, T., OGAWA, H., MIYAJIMA, N., SATA, N. & YAGI, T. 2004. Approach to the mineralogy of the lower mantle by a combined method of a laser-heated diamond anvil cell experiment and analytical electron microscopy. *Physics of the Earth and Planetary Interiors*, 143, 215-221.
- GROCHOLSKI, B., CATALLI, K., SHIM, S.-H. & PRAKAPENKA, V. 2012. Mineralogical effects on the detectability of the postperovskite boundary. *Proceedings of the National Academy of Sciences of the United States of America*, 109, 2275-2279.
- HASHIN, Z. & SHTRIKMAN, S. 1963. A VARIATIONAL APPROACH TO THE THEORY OF THE ELASTIC BEHAVIOUR OF MULTIPHASE MATERIALS. *Journal of the Mechanics and Physics of Solids*, 11, 127-140.
- HIROSE, K. & FEI, Y. W. 2002. Subsolvus and melting phase relations of basaltic composition in the uppermost lower mantle. *Geochimica Et Cosmochimica Acta*, 66, 2099-2108.
- HIROSE, K., TAKAFUJI, N., SATA, N. & OHISHI, Y. 2005. Phase transition and density of subducted MORB crust in the lower mantle. *Earth and Planetary Science Letters*, 237, 239-251.
- IRIFUNE, T., MIYASHITA, M., INOUE, T., ANDO, J., FUNAKOSHI, K. & UTSUMI, W. 2000. High-pressure phase transformation in CaMgSi₂O₆ and implications for origin of ultra-deep diamond inclusions. *Geophysical Research Letters*, 27, 3541-3544.
- IRIFUNE, T. & RINGWOOD, A. E. 1993. PHASE-TRANSFORMATIONS IN SUBDUCTED OCEANIC-CRUST AND BUOYANCY RELATIONSHIPS AT DEPTHS OF 600-800 KM IN THE MANTLE. *Earth and Planetary Science Letters*, 117, 101-110.
- IRIFUNE, T., SUSAKI, J., YAGI, T. & SAWAMOTO, H. 1989. PHASE-TRANSFORMATIONS IN DIOPSIDE CaMgSi₂O₆ AT PRESSURES UP TO 25-GPA. *Geophysical Research Letters*, 16, 187-190.
- IRIFUNE, T. & TSUCHIDA, Y. 2007. Mineralogy of the Earth—Phase transitions and mineralogy of the lower mantle. In: GD, P. & G, S. (eds.) *Treatise on Geophysics, Vol 2 Mineral Physics*.
- JUNG, D. Y. & SCHMIDT, M. W. 2011. Solid solution behaviour of CaSiO₃ and MgSiO₃ perovskites. *Physics and Chemistry of Minerals*, 38, 311-319.
- KAMINSKI, F. 2017. *The Earth's Lower Mantle: Composition and Structure*, Springer International Publishing.
- KAWAI, K. & TSUCHIYA, T. 2015. Small shear modulus of cubic CaSiO₃ perovskite. *Geophysical Research Letters*, 42, 2718-2726.
- KESSON, S. E., FITZ GERALD, J. D. & SHELLEY, J. M. 1998. Mineralogy and dynamics of a pyrolite lower mantle. *Nature*, 393, 252-255.
- KESSON, S. E., FITZ GERALD, J. D., SHELLEY, J. M. G. & WITHERS, R. L. 1995. PHASE-RELATIONS, STRUCTURE AND CRYSTAL-CHEMISTRY OF SOME ALUMINOUS SILICATE PEROVSKITES. *Earth and Planetary Science Letters*, 134, 187-201.
- KRESSE, G. & FURTHMULLER, J. 1996a. Efficiency of ab-initio total energy calculations for metals and semiconductors using a plane-wave basis set. *Computational Materials Science*, 6, 15-50.
- KRESSE, G. & FURTHMULLER, J. 1996b. Efficient iterative schemes for ab initio total-energy calculations using a plane-wave basis set. *Physical Review B*, 54, 11169-11186.

- KRESSE, G. & JOUBERT, D. 1999. From ultrasoft pseudopotentials to the projector augmented-wave method. *Physical Review B*, 59, 1758-1775.
- KUPENKO, I., MCCAMMON, C., SINMYO, R., PRESCHER, C., CHUMAKOV, A. I., KANTOR, A., RUEFFER, R. & DUBROVINSKY, L. 2014. Electronic spin state of Fe,Al-containing MgSiO_3 perovskite at lower mantle conditions. *Lithos*, 189, 167-172.
- MATTERN, E., MATAS, J., RICARD, Y. & BASS, J. 2005. Lower mantle composition and temperature from mineral physics and thermodynamic modelling. *Geophysical Journal International*, 160, 973-990.
- MCNAMARA, A. K. 2019. A review of large low shear velocity provinces and ultra low velocity zones. *Tectonophysics*, 760, 199-220.
- MICHAEL, P. J. & BONATTI, E. 1985. PERIDOTITE COMPOSITION FROM THE NORTH-ATLANTIC - REGIONAL AND TECTONIC VARIATIONS AND IMPLICATIONS FOR PARTIAL MELTING. *Earth and Planetary Science Letters*, 73, 91-104.
- MUIR, J. M. R. & BRODHOLT, J. P. 2016. Ferrous iron partitioning in the lower mantle. *Physics of the Earth and Planetary Interiors*, 257, 12-17.
- O' NEILL, B. & JEANLOZ, R. 1990. EXPERIMENTAL PETROLOGY OF THE LOWER MANTLE - A NATURAL PERIDOTITE TAKEN TO 54 GPa. *Geophysical Research Letters*, 17, 1477-1480.
- OGANOV, A. R. & ONO, S. 2004. Theoretical and experimental evidence for a post-perovskite phase of MgSiO_3 in Earth's D'' layer. *Nature*, 430, 445-448.
- ONO, S. 2008. Experimental constraints on the temperature profile in the lower mantle. *Physics of the Earth and Planetary Interiors*, 170, 267-273.
- ONO, S., KIKEGAWA, T. & IIZUKA, T. 2004. The equation of state of orthorhombic perovskite in a peridotitic mantle composition to 80 GPa: implications for chemical composition of the lower mantle. *Physics of the Earth and Planetary Interiors*, 145, 9-17.
- PRADHAN, G. K., FIQUET, G., SIEBERT, J., AUZENDE, A. L., MORARD, G., ANTONANGELI, D. & GARBARINO, G. 2015. Melting of MORB at core-mantle boundary. *Earth and Planetary Science Letters*, 431, 247-255.
- RICOLLEAU, A., PERRILLAT, J.-P., FIQUET, G., DANIEL, I., MATAS, J., ADDAD, A., MENGUY, N., CARDON, H., MEZOUAR, M. & GUIGNOT, N. 2010. Phase relations and equation of state of a natural MORB: Implications for the density profile of subducted oceanic crust in the Earth's lower mantle. *Journal of Geophysical Research-Solid Earth*, 115.
- RINGWOOD, A. E. 1991. PHASE-TRANSFORMATIONS AND THEIR BEARING ON THE CONSTITUTION AND DYNAMICS OF THE MANTLE. *Geochimica Et Cosmochimica Acta*, 55, 2083-2110.
- SHIM, S. H., GROCHOLSKI, B., YE, Y., ALP, E. E., XU, S. Z., MORGAN, D., MENG, Y. & PRAKAPENKA, V. B. 2017. Stability of ferrous-iron-rich bridgmanite under reducing midmantle conditions. *Proceedings of the National Academy of Sciences of the United States of America*, 114, 6468-6473.
- SHUKLA, G., WU, Z. Q., HSU, H., FLORIS, A., COCCIONI, M. & WENTZCOVITCH, R. M. 2015. Thermoelasticity of Fe^{2+} -bearing bridgmanite. *Geophysical Research Letters*, 42, 1741-1749.
- STIXRUDE, L., LITHGOW-BERTELLONI, C., KIEFER, B. & FUMAGALLI, P. 2007. Phase stability and shear softening in CaSiO_3 perovskite at high pressure. *Physical Review B*, 75.
- SUN, T., ZHANG, D. B. & WENTZCOVITCH, R. M. 2014. Dynamic stabilization of cubic CaSiO_3 perovskite at high temperatures and pressures from ab initio molecular dynamics. *Physical Review B*, 89, 094109-1.
- TAMAI, H. & YAGI, T. 1989. HIGH-PRESSURE AND HIGH-TEMPERATURE PHASE-RELATIONS IN CaSiO_3 AND $\text{CaMgSi}_2\text{O}_6$ AND ELASTICITY OF PEROVSKITE-TYPE CaSiO_3 . *Physics of the Earth and Planetary Interiors*, 54, 370-377.
- THOMSON, A. R., CRICHTON, W. A., BRODHOLT, J. P., WOOD, I. G., SIERSCH, N. C., MUIR, J. M. R., DOBSON, D. P. & HUNT, S. A. 2019. Seismic velocities of CaSiO_3 perovskite can explain LLSVPs in Earth's lower mantle. *Nature*, 572, 643-+.

- VITOS, L., MAGYARI-KOPE, B., AHUJA, R., KOLLAR, J., GRIMVALL, G. & JOHANSSON, B. 2006. Phase transformations between garnet and perovskite phases in the Earth's mantle: A theoretical study. *Physics of the Earth and Planetary Interiors*, 156, 108-116.
- XU, S., SHIM, S.-H. & MORGAN, D. 2015. Origin of Fe³⁺ in Fe-containing, Al-free mantle silicate perovskite. *Earth and Planetary Science Letters*, 409, 319-328.
- ZHANG, Z., STIXRUDE, L. & BRODHOLT, J. 2013. Elastic properties of MgSiO₃-perovskite under lower mantle conditions and the composition of the deep Earth. *Earth and Planetary Science Letters*, 379, 1-12.

Figure Captions:

Figure 1:

Plot of H_{mix} (black lines) for a 50:50 (solid) and a 12.5:87.5 (dashed) mixture of Ca-pv and bdg phases and T_{mix} (red lines) if $\Delta S_{\text{mix}}=0$ and S_{config} is perfect. As can be seen all of these values increase with pressure.

Figure 2 Solubility of Mg in Ca-pv (blue) and Ca in bdg (red) as a function of temperature and pressure (solid lines=25 GPa, dashed=75, dotted=125). The plateau after the graph levels off is the temperature where all ratios of Ca-pv and bdg are miscible into a single phase.

Figure 3: Projected T_{mix} for a pyrolytic mixture with various additional elements against a lower mantle geotherm (Ono, 2008), the coldest possible slab adiabat (Eberle et al., 2002) and an artificial “hot” geotherm representing hot spots in the lower mantle that is the geotherm+500 K. The lines represent Ca%=10 while shading represents Ca% bounds between 7 and 12 which is roughly the Ca% range of pyrolite. Lower Ca% values correspond to lower T_{mix} . Ca% becomes more important as defect elements have stronger effect on T_{mix} . This plot was constructed by calculating T_{mix} for $\text{CaSiO}_3\text{-MgSiO}_3$ at 25, 75 and 125 GPa and adding in the effect of additional elements as determined in Table 3 (with 75 GPa as the average of 25 and 125 GPa effects) and then fitting a curve to these 3 points. These curves have significant approximations in that ΔS_{vib} is not calculated for other elements.

Figure 4: As Figure 3 but for a Harzburgitic mantle (Ca%=3) and with Ca% bounds of 1-3%. The 20% Fe 5% Al component is always below 1000 K and thus is not shown here. In this case the upper bound corresponds to Ca%=3, the lower bound to Ca%=1.

Figure 5: As figure 3 but for a MORB mixture (Ca%=50) and with Ca% bounds of 30-60. Ca% is much less important in this range as configurational entropy dominates- see Fig 2- and thus the bounds are much narrower than in Figure 3. In this case Ca%=50 corresponds to the upper bound and Ca%=60 the lower bound with Ca%=30 near the Ca%=60 bound.

Figure 6: Plot of the change in V_s (solid lines), V_p (dashed lines), V_ϕ (dotted black lines) on converting from a mechanical mixture of Ca-pv and bdg to a single phase calculated directly at Ca%=12.75. These calculations were run at static conditions (~ 0 K) and 25, 75 and 125 GPa. Ca-pv elasticity was determined in the cubic pm3m phase, bdg and the mixed phase in the pbnm phase. To determine elasticity of a mechanical mixture of the two endmembers phase it is necessary to know the geometry of mixing, as we do not that in this case we used the Hashin-Shtikman **bounds REFERENCE** and thus each estimate has an upper and lower bound- the elasticity of the mechanical mixture must be within these bounds.

Table 1: S_{config} (in eV K^{-1} per formula unit) in the mixed phase as a function of Ca%, P and T as well as the ideal value of this in a perfect mixed system.

Table 2 Plot of ΔS_{vib} (in meV/K per f.u.) upon mixing Ca-pv and bdg with two different Ca% values as a function of temperature and pressure.

Table 3: Change in density on forming a mixed phase for Ca%=50 (determined from MD) and 12.5 (extrapolated from MD values at Ca%=25 and 50) at various pressures and temperatures.

Table 4: Effect of various elements on T_{mix} at 25 and 125 GPa with Ca%=10% (Ca%=50 and 90 values are in Table S1 and S2) which is a roughly pyrolytic mixture. Columns are name of the element, site at which that element was placed (A=Mg site, B= Si site, AB= 1 element at each, Int=interstitial), the change in ΔH_{mix} in eV from placing one defect element, proportion of this element in the Ca-pv before mixing (1 is all in Ca-pv, 0 is all in bdg), change in T_{mix} (K) with various amounts of element (in atomic % of bridgmanite). All elements are non-spin polarised except those labelled HS which were run with their standard high spin configuration. 2H represents a water molecule where a Mg has been replaced with 2 Hydrogens in the vacancy. Fe-Al represents a high spin ferric iron replacing a Mg and an Al replacing a Si.

Table 5: Comparison of the effect Ti has on T_{Mix} with different atomic% values as predicted with Table 4 and as calculated fully using MD and configurational entropy calculations.

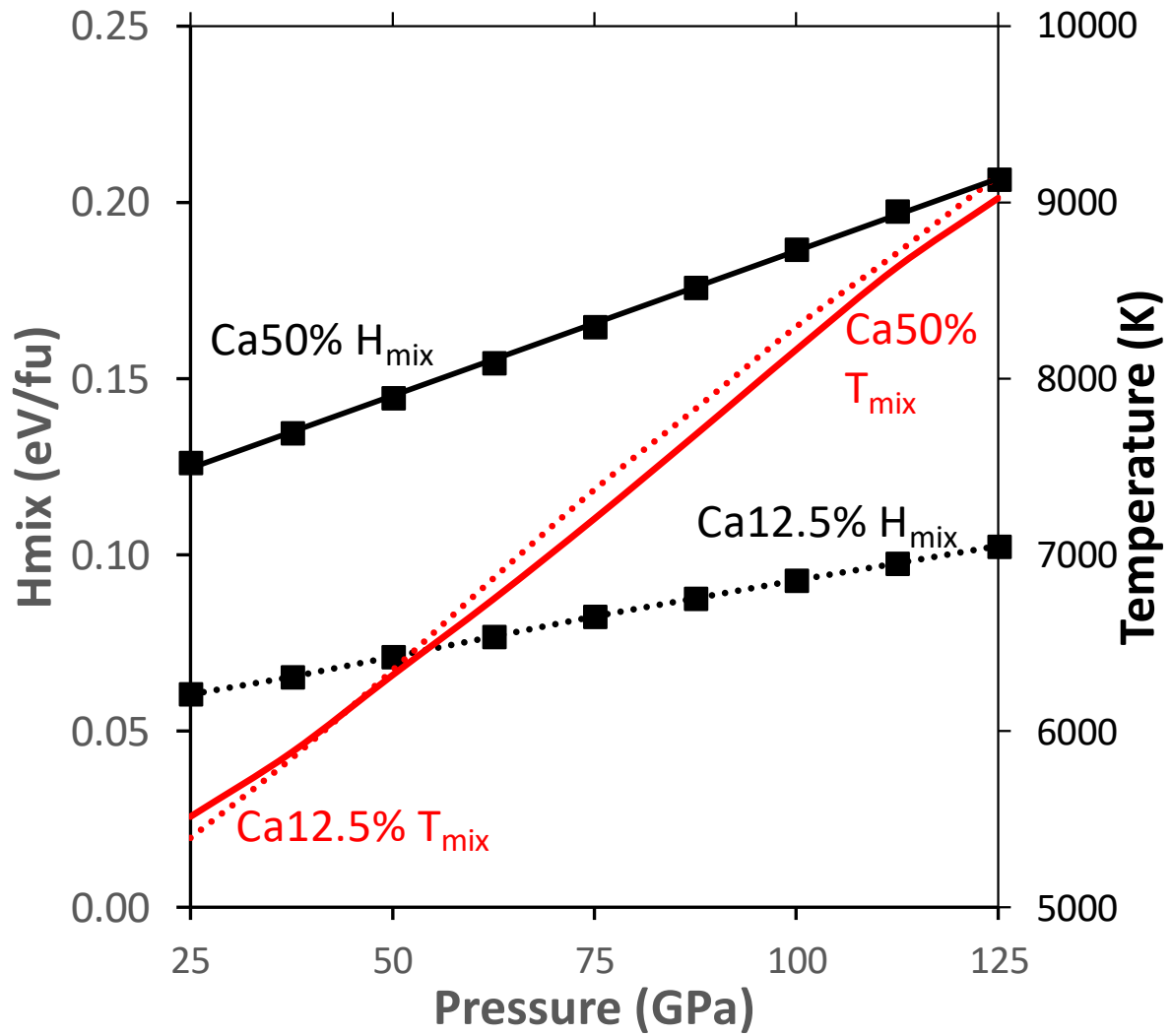


Figure 1:

Plot of H_{mix} (black lines) for a 50:50 (solid) and a 12.5:87.5 (dashed) mixture of Ca-pv and bdg phases and T_{mix} (red lines) if $\Delta S_{mix}=0$ and S_{config} is perfect. As can be seen all of these values increase with pressure.

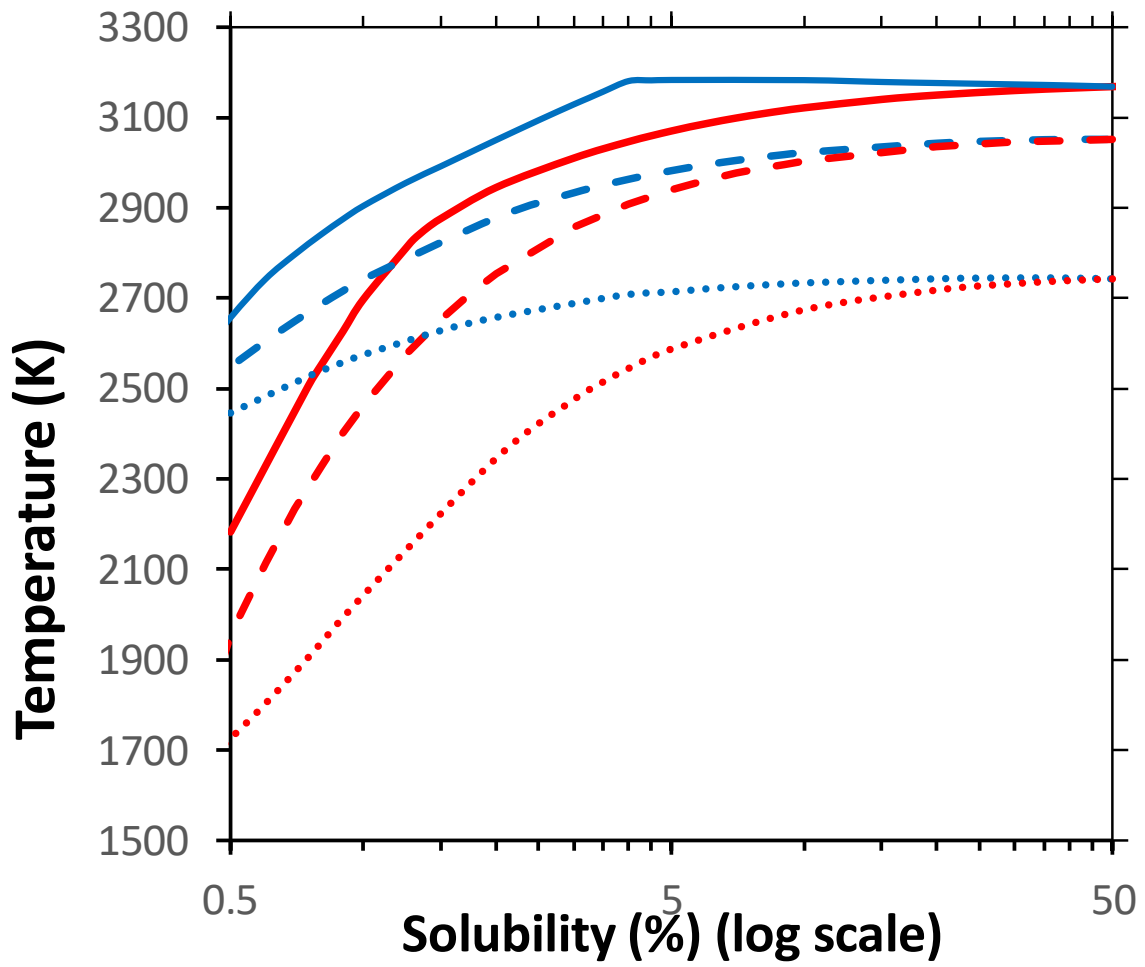


Figure 2 Solubility of Mg in Ca-pv (blue) and Ca in bdg (red) as a function of temperature and pressure (solid lines=25 Gpa, dashed=75, dotted=125). The plateau after the graph levels off is the temperature where all ratios of Ca-pv and bdg are miscible into a single phase.

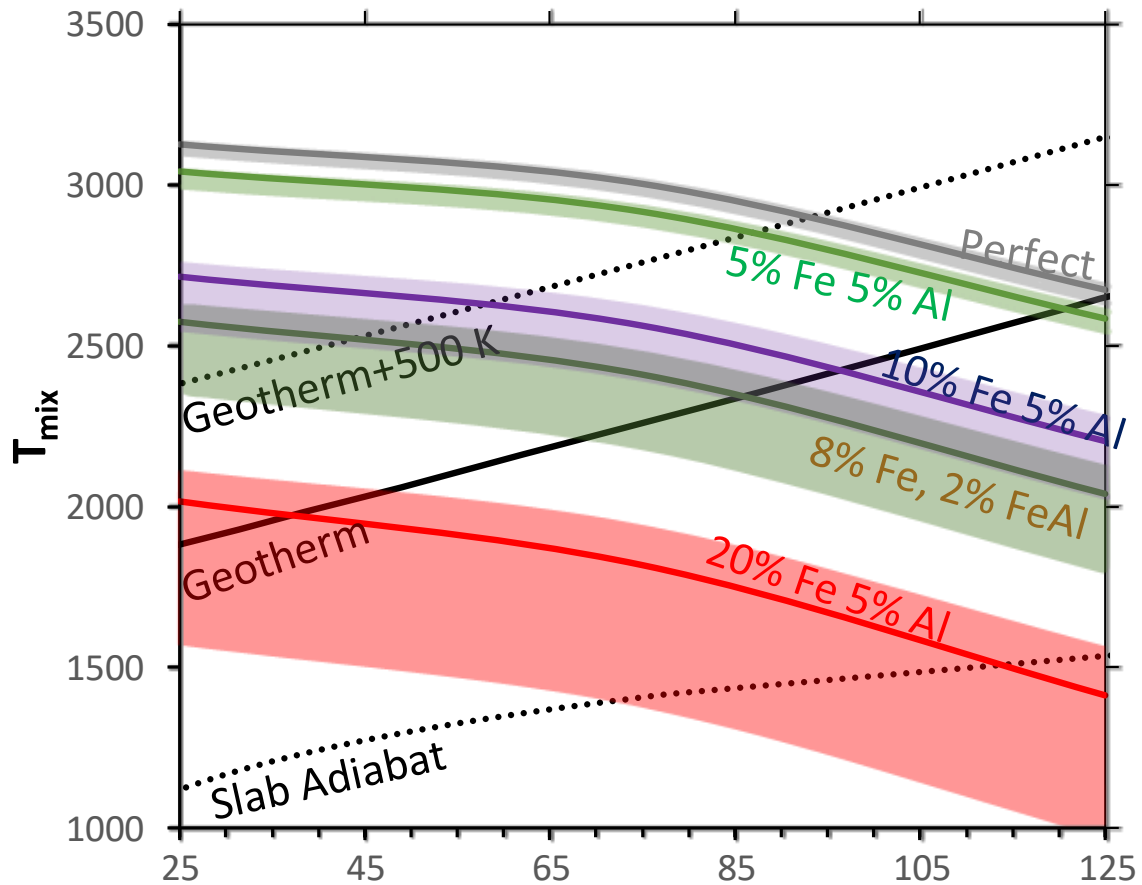


Figure 3: Projected T_{mix} for a pyrolytic mixture with various additional elements against a lower mantle geotherm (Ono, 2008), the coldest possible slab adiabat (Eberle et al., 2002) and an artificial “hot” geotherm representing hot spots in the lower mantle that is the geotherm+500 K. The lines represent $Ca\%=10$ while shading represents $Ca\%$ bounds between 7 and 12 which is roughly the $Ca\%$ range of pyrolite. Lower $Ca\%$ values correspond to lower T_{mix} . $Ca\%$ becomes more important as defect elements have stronger effect on T_{mix} . This plot was constructed by calculating T_{mix} for $CaSiO_3$ - $MgSiO_3$ at 25, 75 and 125 GPa and adding in the effect of additional elements as determined in Table 3 (with 75 GPa as the average of 25 and 125 GPa effects) and then fitting a curve to these 3 points. These curves have significant approximations in that ΔS_{vib} is not calculated for other elements.

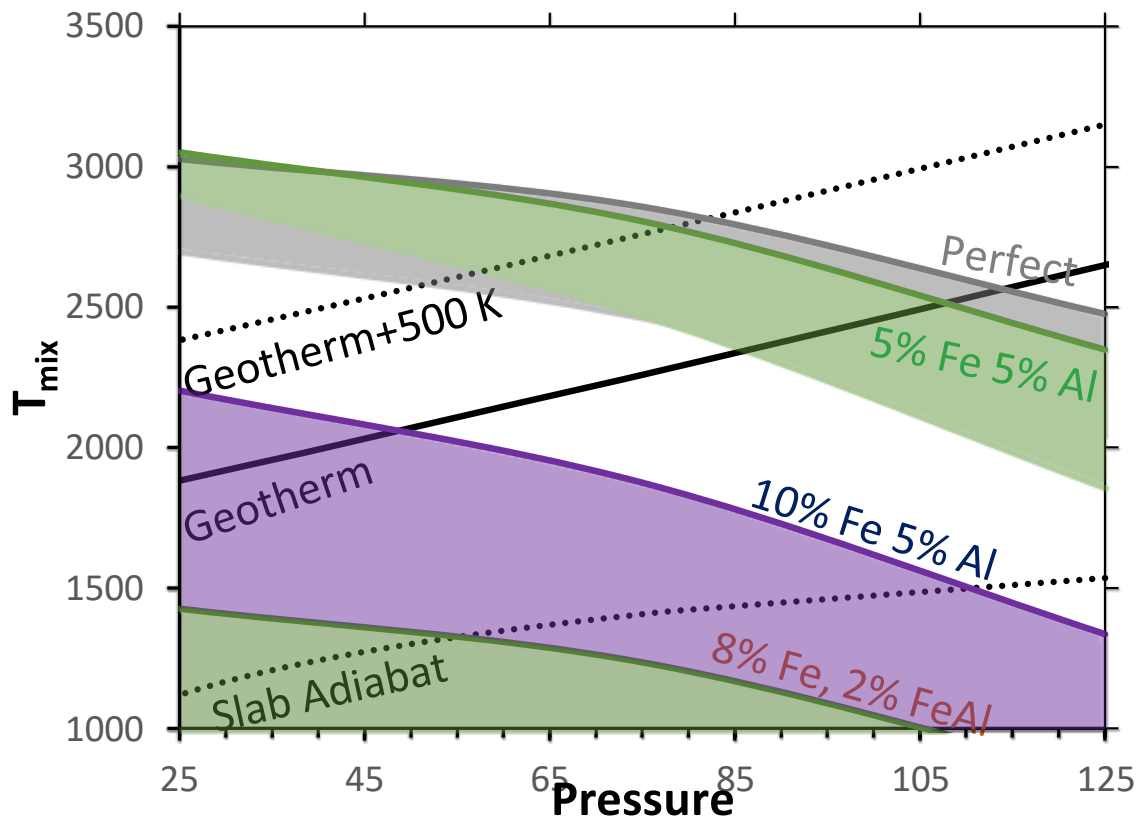


Figure 4: As Figure 3 but for a Harzburgitic mantle ($Ca\%=3$) and with $Ca\%$ bounds of 1-3%. The 20% Fe 5% Al component is always below 1000 K and thus is not shown here. In this case the upper bound corresponds to $Ca\%=3$, the lower bound to $Ca\%=1$.

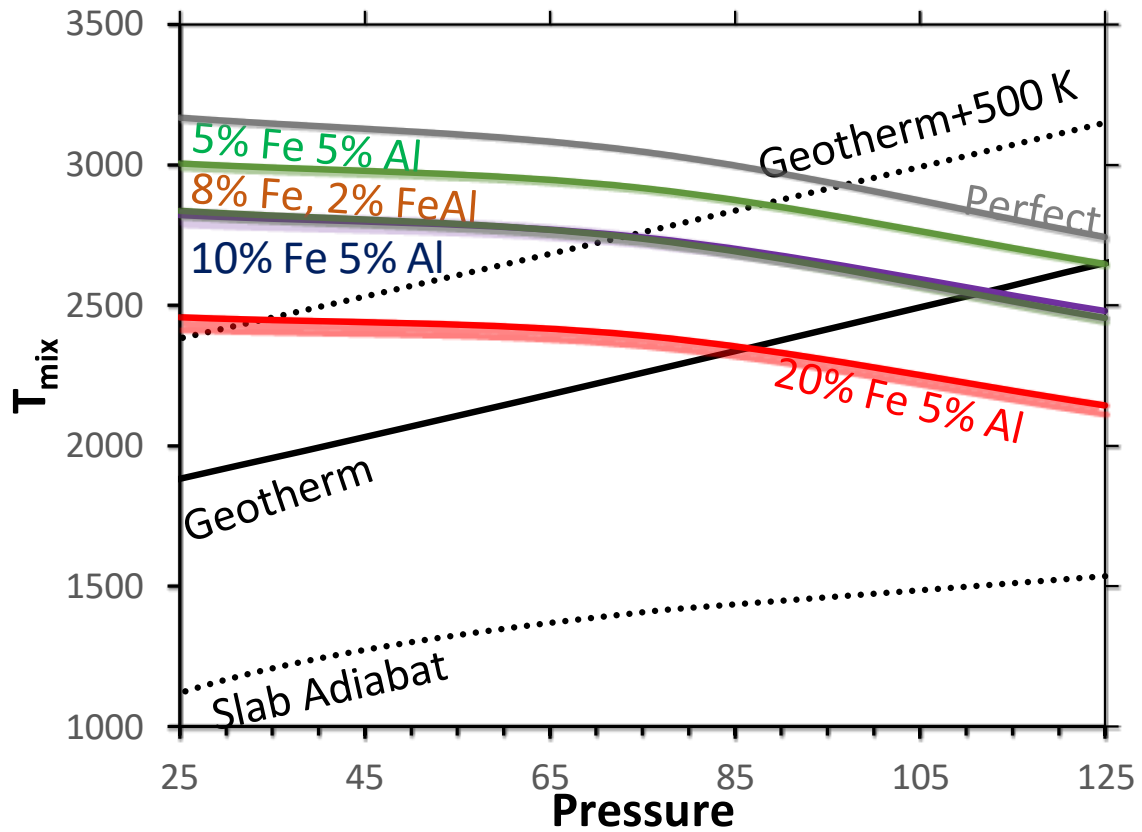


Figure 5: As figure 3 but for a MORB mixture ($\text{Ca}\%=50$) and with $\text{Ca}\%$ bounds of 30-60. $\text{Ca}\%$ is much less important in this range as configurational entropy dominates- see Fig 2- and thus the bounds are much narrower than in Figure 3. In this case $\text{Ca}\%=50$ corresponds to the upper bound and $\text{Ca}\%=60$ the lower bound with $\text{Ca}\%=30$ near the $\text{Ca}\%=60$ bound.

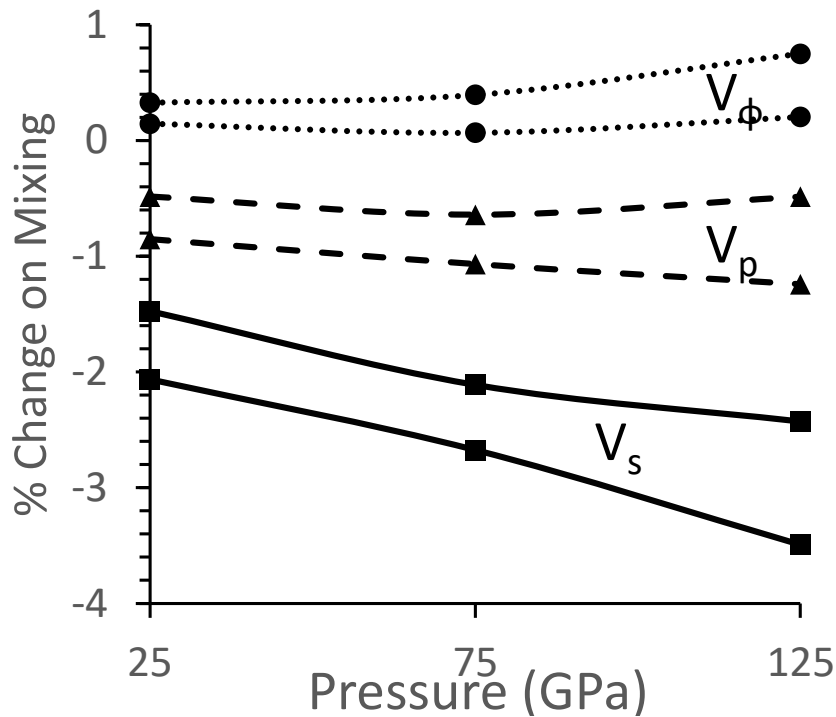


Figure 6: Plot of the change in V_s (solid lines), V_p (dashed lines), V_ϕ (dotted black lines) on converting from a mechanical mixture of Ca-pv and bdg to a single phase calculated directly at Ca%=12.75. These calculations were run at static conditions (~ 0 K) and 25, 75 and 125 GPa. Ca-pv elasticity was determined in the cubic pm3m phase, bdg and the mixed phase in the pbnm phase. To determine elasticity of a mechanical mixture of the two endmembers phase it is necessary to know the geometry of mixing, as we do not that in this case we used the Hashin-Shtikman **bounds REFERENCE** and thus each estimate has an upper and lower bound- the elasticity of the mechanical mixture must be within these bounds.

| | Ca% | 100 | 75 | 50 | 25 | 12.5 | 0 |
|---------|--------|-----|-----------------------|-----------------------|-----------------------|-----------------------|---|
| 25 Gpa | 1000 K | 0 | 2.89×10^{-5} | 4.00×10^{-5} | 3.35×10^{-5} | 2.06×10^{-5} | 0 |
| | 2000 | 0 | 3.40×10^{-5} | 4.34×10^{-5} | 3.56×10^{-5} | 2.19×10^{-5} | 0 |
| | 3000 | 0 | 3.51×10^{-5} | 4.58×10^{-5} | 3.57×10^{-5} | 2.22×10^{-5} | 0 |
| 75 GPa | 1000 K | 0 | 3.16×10^{-5} | 4.12×10^{-5} | 3.45×10^{-5} | 2.12×10^{-5} | 0 |
| | 2000 | 0 | 3.47×10^{-5} | 4.40×10^{-5} | 3.57×10^{-5} | 2.32×10^{-5} | 0 |
| | 3000 | 0 | 3.53×10^{-5} | 4.58×10^{-5} | 3.58×10^{-5} | 2.37×10^{-5} | 0 |
| 125 Gpa | 1000 K | 0 | 3.42×10^{-5} | 4.23×10^{-5} | 3.55×10^{-5} | 2.18×10^{-5} | 0 |
| | 2000 | 0 | 3.54×10^{-5} | 4.46×10^{-5} | 3.58×10^{-5} | 2.44×10^{-5} | 0 |
| | 3000 | 0 | 3.55×10^{-5} | 4.57×10^{-5} | 3.59×10^{-5} | 2.51×10^{-5} | 0 |
| Perfect | | 0 | 3.59×10^{-5} | 4.58×10^{-5} | 3.59×10^{-5} | 2.24×10^{-5} | 0 |

Table 1: S_{Config} (in eV K^{-1} per formula unit) in the mixed phase as a function of Ca%, P and T as well as the ideal value of this in a perfect mixed system.

| | | 1000 K | 2000 | 3000 |
|--------|--------|--------|-------|-------|
| 25 GPa | Ca=50% | 0.040 | 0.015 | 0.041 |
| | 25% | -0.033 | 0.011 | 0.031 |
| 75 | 50% | 0.067 | 0.075 | 0.069 |
| | 25% | -0.033 | 0.041 | 0.044 |
| 125 | 50% | -0.094 | 0.099 | 0.132 |
| | 25% | -0.033 | 0.074 | 0.099 |

Table 2 Plot of ΔS_{vib} (in meV/K per f.u.) upon mixing Ca-pv and bdg with two different Ca% values as a function of temperature and pressure.

| | Ca%=12.5 | | | Ca%=50 | | |
|--------|----------|-------|-------|--------|-------|-------|
| | 25 GPa | 75 | 125 | 25 GPa | 75 | 125 |
| 1000 K | -0.15 | -0.17 | -0.18 | -0.59 | -0.69 | -0.73 |
| 2000 | -0.19 | -0.19 | -0.19 | -0.76 | -0.77 | -0.75 |
| 3000 | -0.25 | -0.23 | -0.19 | -0.98 | -0.93 | -0.76 |

Table 3: Change in density on forming a mixed phase for Ca%=50 (determined from MD) and 12.5 (extrapolated from MD values at Ca%=25 and 50) at various pressures and temperatures.

| Element | Site | 25 GPa | | | | | 125 GPa | | | | |
|-----------|------|-------------------------|----------|-----------|------------|-------------|-------------------------|----------|-----------|------------|-------------|
| | | ΔH_{mix} | K | 0.10% | 1 | 10 | ΔH_{mix} | K | 0.10% | 1 | 10 |
| 2H | A | 0.11 | 0 | 2 | 16 | 148 | 0.95 | 0 | 13 | 134 | 1224 |
| He | Int | -0.27 | 1 | -23 | -233 | -1883 | 0.07 | 1 | -7 | -70 | -628 |
| Ne | Int | -0.86 | 1 | -39 | -389 | -3453 | -0.90 | 1 | -21 | -213 | -1839 |
| Li(I) | A | 0.28 | 0 | 6 | 60 | 538 | 0.76 | 0 | 11 | 106 | 981 |
| Na(I) | A | -0.42 | 0 | -12 | -125 | -1412 | -0.53 | 0 | -9 | -86 | -883 |
| K(I) | A | -0.10 | 1 | -32 | -305 | -2057 | -0.16 | 1 | -17 | -162 | -1301 |
| Be(II) | A | 0.18 | 0 | 3 | 34 | 311 | 1.17 | 0 | 17 | 166 | 1505 |
| Cu(II) | A | -0.14 | 0 | -5 | -51 | -526 | -0.38 | 0 | -6 | -64 | -646 |
| Ni(II) | A | -0.39 | 0 | -11 | -116 | -1292 | -0.47 | 0 | -8 | -77 | -791 |
| Zn(II) | A | -0.13 | 0 | -5 | -47 | -477 | -0.43 | 0 | -7 | -71 | -722 |
| Co(II) | A | -0.42 | 0 | -12 | -124 | -1400 | -0.55 | 0 | -9 | -89 | -921 |
| Fe(II) | A | -0.31 | 0 | -9 | -95 | -1029 | -0.48 | 0 | -8 | -79 | -811 |
| Fe(II)HS | A | -0.20 | 0 | -7 | -65 | -682 | -0.47 | 0 | -8 | -76 | -783 |
| V(II) | A | -0.26 | 0 | -8 | -82 | -875 | -0.45 | 0 | -7 | -74 | -761 |
| Cr(II) | A | 0.09 | 0 | 1 | 9 | 82 | -0.23 | 0 | -4 | -41 | -417 |
| Mn(II) | A | 0.25 | 0 | 5 | 52 | 473 | 0.14 | 0 | 1 | 15 | 140 |
| Sc(II) | A | -0.22 | 1 | -35 | -336 | -2244 | -0.07 | 1 | -15 | -150 | -1216 |
| Sc(II) HS | A | -0.26 | 1 | -36 | -347 | -2313 | -0.60 | 1 | -1 | -7 | -67 |
| Sr(II) | A | 0.51 | 1 | -16 | -153 | -1193 | 0.70 | 1 | -4 | -39 | -491 |
| Ba(II) | A | 0.98 | 1 | -4 | -38 | -581 | 1.38 | 1 | 6 | 57 | 114 |
| B(III) | AB | 0.62 | 1 | 15 | 147 | 1253 | -0.77 | 1 | -12 | -123 | -1294 |
| Al(III) | AB | 0.24 | 0 | 5 | 48 | 439 | 0.43 | 0 | 6 | 58 | 550 |
| Cr(III) | AB | -0.17 | 1 | <u>0</u> | <u>-4</u> | <u>-44</u> | 0.07 | 1 | <u>0</u> | <u>5</u> | <u>44</u> |
| Cr(III)Hs | AB | 0.14 | 1 | <u>2</u> | <u>23</u> | <u>218</u> | -0.15 | 1 | <u>-3</u> | <u>-29</u> | <u>-289</u> |
| Ga(III) | AB | 0.13 | 0 | 2 | 20 | 185 | 0.34 | 0 | 4 | 44 | 419 |
| Fe(III) | AB | 0.79 | 0 | 19 | 188 | 1569 | 1.03 | 0 | 15 | 146 | 1337 |
| Fe(III)HS | AB | 0.01 | 0 | -1 | -10 | -96 | 0.18 | 0 | 2 | 20 | 189 |
| Sc(III) | AB | -0.20 | 0 | -6 | -65 | -673 | -0.07 | 0 | -2 | -17 | -167 |
| In(III) | AB | -0.07 | 0 | -3 | -32 | -322 | 0.17 | 0 | 2 | 19 | 182 |
| Fe-Al | AB | 0.02 | 0 | -1 | -7 | -74 | 0.00 | 0 | -1 | -7 | -71 |
| C 4+ | B | -0.51 | 1 | -15 | -148 | -1753 | -0.08 | 0 | -2 | -19 | -193 |
| S 4+ | B | -0.45 | 0 | -13 | -133 | -1530 | -0.21 | 0 | -4 | -38 | -387 |
| Ge4+ | B | -0.17 | 0 | -6 | -57 | -587 | -0.09 | 0 | -2 | -20 | -204 |
| Sn4+ | B | -0.51 | 0 | -15 | -150 | -1780 | -0.38 | 0 | -6 | -63 | -645 |
| Ti4+ | B | -0.07 | 1 | -3 | -32 | -329 | -0.26 | 0 | -4 | -45 | -452 |

Table 4: Effect of various elements on T_{mix} at 25 and 125 GPa with Ca%=10% (Ca%=50 and 90 values are in Table S1 and S2) which is a roughly pyrolytic mixture. Columns are name of the element, site at which that element was placed (A=Mg site, B= Si site, AB= 1 element at each, Int=interstitial), the change in ΔH_{mix} in eV from placing one defect element, proportion of this element in the Ca-pv before mixing (1 is all in Ca-pv, 0 is all in bdg), change in T_{mix} (K) with various amounts of element (in

atomic % of bridgmanite). All elements are non-spin polarised except those labelled HS which were run with their standard high spin configuration. 2H represents a water molecule where a Mg has been replaced with 2 Hydrogens in the vacancy. Fe-Al represents a high spin ferric iron replacing a Mg and an Al replacing a Si.

| | | 0.1 % | 1 | 10 |
|---------|------------|-------|-----|------|
| 25 GPa | Predicted | -3 | -32 | -329 |
| | Calculated | -9 | -93 | -582 |
| 125 GPa | Predicted | -4 | -45 | -452 |
| | Calculated | -3 | -29 | -251 |

Table 5: Comparison of the effect Ti has on T_{Mix} with different atomic% values as predicted with Table 4 and as calculated fully using MD and configurational entropy calculations.

Supplementary Information for the miscibility of Calcium Silicate Perovskite and Bridgmanite: A
single phase perovskite in hot, iron-rich regions

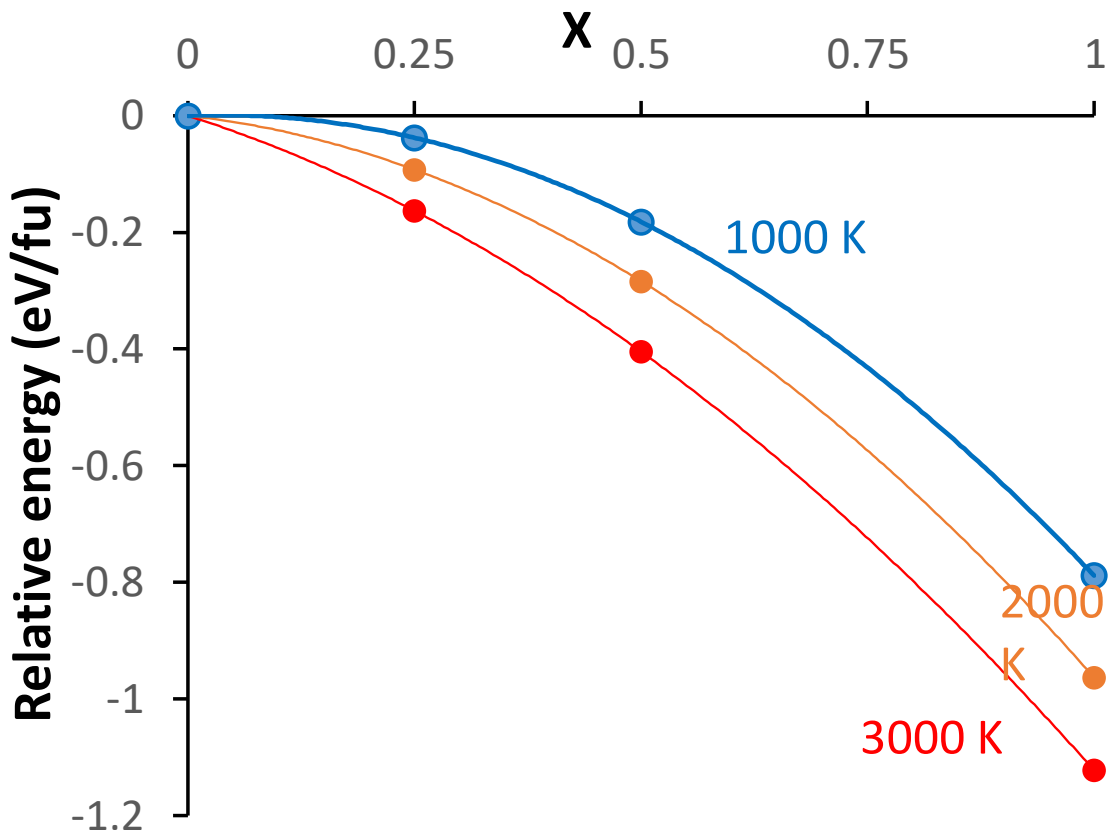


Figure S1: Plot of the energy of different compositions of $\text{Ca}_x\text{Mg}_{1-x}\text{SiO}_3$ relative to the energy of MgSiO_3 at 25 GPa. The plotted line was drawn with $x=0, 0.5$ and 1 and $x=0.25$ was determined independently. This shows that a polynomial fit is appropriate for these phases except maybe at extreme values of x . Similar behaviour was observed at 75 and 125 GPa.

| Element | Site | 25 GPa | | | | 125 GPa | | | |
|-----------|------|----------|-----------|------------|-------------|----------|-----------|------------|-------------|
| | | K | 0.10% | 1 | 10 | K | 0.10% | 1 | 10 |
| 2H | A | 0 | -1 | -7 | -77 | 0 | 4 | 42 | 389 |
| He | Int | 1 | -4 | -45 | -446 | 1 | 0 | -5 | -50 |
| Ne | Int | 1 | -10 | -103 | -1078 | 1 | -6 | -57 | -581 |
| Li(I) | A | 0 | 1 | 9 | 78 | 0 | 3 | 32 | 297 |
| Na(I) | A | 0 | -6 | -60 | -603 | 0 | -4 | -37 | -373 |
| K(I) | A | 1 | -3 | -28 | -277 | 1 | -2 | -17 | -175 |
| Be(II) | A | 0 | 0 | -1 | -13 | 0 | 5 | 53 | 497 |
| Cu(II) | A | 0 | -3 | -33 | -324 | 0 | -3 | -29 | -292 |
| Ni(II) | A | 0 | -6 | -56 | -569 | 0 | -3 | -34 | -342 |
| Zn(II) | A | 0 | -3 | -31 | -307 | 0 | -3 | -32 | -318 |
| Co(II) | A | 0 | -6 | -59 | -600 | 0 | -4 | -38 | -386 |
| Fe(II) | A | 0 | -5 | -49 | -489 | 0 | -3 | -35 | -349 |
| Fe(II)HS | A | <u>0</u> | <u>-4</u> | <u>-38</u> | <u>-377</u> | <u>0</u> | <u>-3</u> | <u>-34</u> | <u>-339</u> |
| V(II) | A | 0 | -4 | -44 | -440 | 0 | -3 | -33 | -332 |
| Cr(II) | A | 0 | -1 | -10 | -102 | 0 | -2 | -21 | -212 |
| Mn(II) | A | 0 | 1 | 6 | 52 | 0 | 0 | -1 | -14 |
| Sc(II) | A | 1 | -4 | -40 | -397 | 1 | -1 | -13 | -128 |
| Sc(II) HS | A | 1 | -4 | -44 | -442 | 1 | -1 | -9 | -89 |
| Sr(II) | A | 1 | 3 | 31 | 280 | 1 | 3 | 28 | 267 |
| Ba(II) | A | 1 | 8 | 76 | 675 | 1 | 6 | 64 | 594 |
| B(III) | AB | 1 | 20 | 150 | 990 | 1 | 2 | 0 | -263 |
| Al(III) | AB | 0 | 16 | 112 | 629 | 0 | 9 | 65 | 417 |
| Cr(III) | AB | 1 | 14 | 93 | 431 | 1 | 7 | 46 | 224 |
| Cr(III)Hs | AB | 1 | 15 | 103 | 537 | 1 | 6 | 34 | 99 |
| Ga(III) | AB | 0 | 15 | 102 | 524 | 0 | 8 | 60 | 367 |
| Fe(III) | AB | 0 | 21 | 166 | 1137 | 0 | 12 | 97 | 727 |
| Fe(III)HS | AB | <u>0</u> | <u>14</u> | <u>91</u> | <u>411</u> | <u>0</u> | <u>7</u> | <u>51</u> | <u>279</u> |
| Sc(III) | AB | 0 | 12 | 70 | 194 | <u>0</u> | 6 | 38 | 144 |
| In(III) | AB | 0 | 13 | 82 | 323 | 0 | 7 | 51 | 276 |
| Fe-Al | AB | <u>0</u> | <u>14</u> | <u>91</u> | <u>420</u> | <u>0</u> | <u>6</u> | <u>42</u> | <u>180</u> |
| C 4+ | B | 1 | 7 | 23 | -329 | 0 | 5 | 30 | 50 |
| S 4+ | B | 0 | 8 | 29 | -267 | 0 | 5 | 23 | -21 |
| Ge4+ | B | 0 | 11 | 57 | 39 | 0 | 5 | 30 | 46 |
| Sn4+ | B | 0 | 7 | 23 | -336 | 0 | 4 | 14 | -114 |
| Ti4+ | B | 1 | 12 | 66 | 134 | 0 | 4 | 21 | -45 |

Table S1: Effect of various elements on T_{mix} at 25 and 125 GPa with Ca%=50%. Columns are name of the element, site at which that element was placed (A=Mg site, B= Si site, AB= 1

element at each, Int=interstitial), the change in ΔH_{mix} in eV from placing one defect element, proportion of this element in the Ca-pv before mixing (1 is all in Ca-pv, 0 is all in bdg), change in T_{mix} (K) with various amounts of element (in atomic % of bridgmanite). All elements are non-spin polarised except those labelled HS which were run with their standard high spin configuration. 2H represents a water molecule where a Mg has been replaced with 2 Hydrogens in the vacancy.

| Element | Site | 25 GPa | | | | 125 GPa | | | |
|-----------|------|----------|-----------|------------|-------------|----------|-----------|------------|-------------|
| | | K | 0.10% | 1 | 10 | K | 0.10% | 1 | 10 |
| 2H | A | 0 | 0 | -3 | -36 | 0 | 12 | 121 | 1067 |
| He | Int | 1 | -76 | -547 | -2319 | 1 | -32 | -228 | -1063 |
| Ne | Int | 1 | -91 | -697 | -3344 | 1 | -46 | -365 | -2099 |
| Li(I) | A | 0 | 4 | 40 | 351 | 0 | 10 | 94 | 841 |
| Na(I) | A | 0 | -14 | -145 | -1556 | 0 | -9 | -94 | -958 |
| K(I) | A | 1 | -3 | -27 | -277 | 1 | -2 | -25 | -250 |
| Be(II) | A | 0 | 1 | 14 | 125 | 0 | 16 | 153 | 1328 |
| Cu(II) | A | 0 | -7 | -71 | -699 | 0 | -7 | -72 | -722 |
| Ni(II) | A | 0 | -14 | -136 | -1441 | 0 | -9 | -85 | -866 |
| Zn(II) | A | 0 | -7 | -66 | -651 | 0 | -8 | -79 | -797 |
| Co(II) | A | 0 | -14 | -144 | -1544 | 0 | -10 | -97 | -996 |
| Fe(II) | A | 0 | -11 | -115 | -1188 | 0 | -9 | -87 | -886 |
| Fe(II)HS | A | 0 | -9 | -85 | -851 | 0 | -8 | -84 | -858 |
| V(II) | A | 0 | -10 | -102 | -1040 | 0 | -8 | -83 | -837 |
| Cr(II) | A | 0 | -1 | -10 | -101 | 0 | -5 | -50 | -496 |
| Mn(II) | A | 0 | 3 | 33 | 286 | 0 | 1 | 5 | 45 |
| Sc(II) | A | 1 | -6 | -59 | -633 | 1 | -1 | -12 | -118 |
| Sc(II) HS | A | 1 | -7 | -71 | -771 | 1 | -2 | -16 | -155 |
| Sr(II) | A | 1 | 13 | 130 | 1162 | 1 | 10 | 101 | 938 |
| Ba(II) | A | 1 | 25 | 249 | 2061 | 1 | 20 | 198 | 1747 |
| B(III) | AB | 1 | 13 | 128 | 1064 | 1 | -13 | -130 | -1377 |
| Al(III) | AB | 0 | 3 | 29 | 252 | 0 | 5 | 47 | 435 |
| Cr(III) | AB | 1 | -2 | -24 | -226 | 1 | 0 | -5 | -48 |
| Cr(III)Hs | AB | 1 | 0 | 4 | 33 | 1 | -4 | -38 | -371 |
| Ga(III) | AB | 0 | 0 | 0 | 1 | 0 | 3 | 34 | 310 |
| Fe(III) | AB | 0 | 17 | 170 | 1380 | 0 | 14 | 134 | 1172 |
| Fe(III)HS | AB | 0 | -3 | -29 | -277 | 0 | 1 | 10 | 91 |
| Sc(III) | AB | 0 | -8 | -85 | -843 | 0 | -3 | -26 | -252 |
| In(III) | AB | 0 | -5 | -52 | -500 | 0 | 1 | 9 | 84 |
| Fe-Al | AB | 0 | -3 | -27 | -255 | 0 | -2 | -16 | -159 |
| C 4+ | B | 1 | -17 | -168 | -1878 | 0 | -3 | -28 | -277 |
| S 4+ | B | 0 | -15 | -153 | -1667 | 0 | -5 | -47 | -466 |
| Ge4+ | B | 0 | -8 | -77 | -758 | 0 | -3 | -29 | -288 |
| | | | | | - | | | | |
| Sn4+ | B | 0 | -17 | -170 | 1903 | 0 | -7 | -72 | -721 |
| Ti4+ | B | 1 | -5 | -52 | -506 | 0 | -5 | -53 | -531 |

Table S2: As Table S1 but with Ca%=90.

